# Dynamical instability and transport peak of chiral matter from holography

Pei Zheng,[1,2,*] Yidian Chen,[3,†] Danning Li,[4,‡] Mei Huang,[1,§] and Yu-xin Liu[2,5,‖]

[1]*School of Nuclear Science and Technology, University of Chinese Academy of Sciences, Beijing 100049, China*

[2]*Department of Physics and State Key Laboratory of Nuclear Physics and Technology, Peking University, Beijing 100871, China*

[3]*School of Physics, Hangzhou Normal University, Hangzhou, 311121, China*

[4]*Department of Physics and Siyuan Laboratory, Jinan University, Guangzhou 510632, China*

[5]*Center for High Energy Physics, Peking University, Beijing 100871, China*

(Received 4 August 2025; accepted 16 September 2025; published 10 October 2025)

We study dynamical properties of strongly coupled chiral matter by using the holographic method. We demonstrate, at both linear and nonlinear levels, that perturbations on thermodynamically unstable backgrounds within the spinodal region of chiral first-order phase transitions exhibit dynamic instability. The corresponding magnitude of dynamic instability can be characterized by the critical momentum. Furthermore, we found that, within a certain temperature range, the quasinormal-mode spectrum contains purely imaginary diffusive modes. As spatial momentum increases, a transition occurs in the system's long-time dynamics. The dominant contribution shifts from diffusive mode to propagating mode. When the diffusive mode becomes dominant, the spectral function exhibits a transport peak structure in the low-frequency region. A heuristic argument suggests that this particular transition can be related to the chiral symmetry breaking and restoration.

DOI: 10.1103/mxkj-lcnn

## I. INTRODUCTION

Research on the properties of strong interaction matter has consistently remained a highly active field in theoretical physics. Due to the strong-coupling nature of quantum chromodynamics (QCD) describing strong interactions in the low-energy region, commonly employed perturbative approaches become inapplicable. Since issues of primary concern, such as spontaneous breaking of chiral symmetry and color confinement, are intrinsically linked to low-energy scale physics, in-depth investigation of these phenomena necessitates the development of appropriate nonperturbative field theoretic approaches. Although some methods based on functional integral have made significant progress in studying different aspects of QCD matter [1,2], current research on the dynamical behavior of strongly coupled matter remains insufficient in both systematic rigor and comprehensive scope, as existing functional methods encounter certain difficulties in addressing dynamical issues.

Holographic anti–de Sitter/conformal field theory (AdS/CFT) correspondence [3–6] (see [7] for a review) provides a suitable tool to study strongly coupled systems. This correspondence asserts that string theories lived on (asymptotically) anti–de Sitter spacetime are dual to some quantum field theories in lower dimension. In the low-energy limit, the string theories can be described by appropriate classical supergravity theories. So the problems in quantum field theories can be mapped to problems in classical gravity theories. One of the incredible features is that such duality is the so-called strong/weak duality. To illustrate, physical information in strongly coupled field theories is encoded in weakly coupled gravitational theories by using such duality. This implies that nonperturbative features of strongly coupled field theoretic systems can be extracted by directly studying weakly coupled gravitational theories.

Based on AdS/CFT correspondence, small perturbations of gravity background are interpreted as small perturbations in the dual field theory. This particular situation in holographic theory can be made more precise by checking spectrum of the so-called quasinormal modes of (asymptotically) AdS spacetime. Typically, quasinormal modes are solutions to linearized equation of motions satisfied by all kinds of fluctuations [8–11]. In particular, the boundary conditions should be chosen specifically. Considering the

*Contact author: zhengp@stu.pku.edu.cn
†Contact author: chenyidian@hznu.edu.cn
‡Contact author: lidanning@jnu.edu.cn
§Contact author: huangmei@ucas.ac.cn
‖Contact author: yxliu@pku.edu.cn

*Published by the American Physical Society under the terms of the Creative Commons Attribution 4.0 International license. Further distribution of this work must maintain attribution to the author(s) and the published article's title, journal citation, and DOI. Funded by SCOAP³.*

fact that the future horizon do not emit radiation classically, one choose the incoming waves at the future horizon only. Consequently, the associated boundary value problem becomes non-Hermitian and the corresponding eigenvalues are complex. From the dual field theory perspective, these quasinormal modes can be directly related to the poles of retarded Green's functions [12].

From the gravity perspective, Gregory and Laflamme has already found that there exists a classical instability of higher dimensional black string/brane solutions, which is usually referred to the Gregory-Laflamme (GL) instability [13,14]. In the AdS/CFT correspondence, GL instability rooted in classical gravitational frameworks has acquired novel physical significance. A natural interpretation is that the dual field theory exhibits corresponding dynamical instability. Typically, there is a thermodynamic instability in the field theory at finite temperature, like the spinodal region of a first-order phase transition. Gubser and Mitra naturally conjectured that the system with locally thermodynamical instability will induce dynamical instability [15,16]. The conjecture linking thermodynamic and dynamical properties has been validated in subsequent studies across diverse theoretical frameworks [17–20]. Furthermore, from an alternative perspective grounded in phenomenological consideration, potential dynamical instabilities in strongly coupled chiral QCD matter can also be explored based on the aforementioned conjecture. Regarding the importance of dynamical instabilities manifested in QCD matter, a case in point is that the instabilities of quark-gluon plasma (QGP) are believed to play an important role in the early stages of QGP equilibration [21–24]. Besides, the so-called spatially modulated phase [25,26] is found to be indicated by some dynamical instability of the typical homogeneous QGP phase [27–29]. Owing to all these considerations, the fundamental motivation of this work can be summarized as investigating the potential dynamical instability of QCD chiral matter and meanwhile, examining the validity of the Gubser-Mitra conjecture within this specific physical context.

The paper is organized as follows. In Sec. II, we briefly introduce the model used in this model and related chiral phase transition behaviors. In Sec. IV, we study the dynamical properties of chiral system in the spinodal region of first-order chiral phase transition either in linear perturbation level or in full nonlinear evolution level. Some interesting transition behavior is also observed while studying the quasinormal spectrum. In Sec. V, we investigate such diffusion-to-sound transition by calculating quasinormal modes and also corresponding spectral functions. In Sec. VI, we provide a summary and further discussion.

## II. BASIC HOLOGRAPHIC MODEL SETUP AND CHIRAL PHASE TRANSITION

Within the holographic framework, the hard-wall and soft-wall AdS/QCD models were first proposed in [30,31]. From bottom-up perspective, the 4D global symmetry $SU(N_f)_L \times SU(N_f)_R$ of chiral system is directly promoted to 5D gauge symmetry of the corresponding bulk system. By incorporating desired symmetry structure, these effective models are suitable to study problems related to the spontaneous symmetry breaking of chiral symmetry. Based on the hard-wall model, a quadratic dilaton model was introduced in the soft-wall model to describe the linear trajectory of the higher excitations. At finite temperature, after introducing an additional scale relevant for chiral dynamics, the phase diagram obtained from the soft-wall model [32–39] was shown to qualitatively agree with the so-called Columbia plot obtained by combining lattice simulations and other effective methods. In addition to the order parameter, the thermal properties of hadrons, in particular of the Goldstone bosons, were shown to qualitatively agree [40–42] with the four-dimensional finite temperature chiral perturbation theory [43]. Besides the equilibrium studies, it is also very convenient to extend this model to study the nonequilibrium phase transition. Near the second order transition, a nontrivial dynamic phenomena called prethermalization was shown to appear in the intermediate time [44–46]. But the dynamic instabilities close to the first order phase transition was rarely studied within this model. Thus, it is still interesting to study the dynamic properties of the first-order phase transition in this model.

### A. The nonlinear soft-wall model

In this work, we use the conventions of [31] and write the 5D action of the nonlinear soft-wall model as

$$S = -\int d^5x\sqrt{-g}e^{-\Phi} \times \mathrm{Tr}\left[|D_m X|^2 + V_X(X) + \frac{1}{4g_5^2}(F_L^2 + F_R^2)\right], \quad (1)$$

where

$$F_{mn}^{L/R} = \partial_m A_n^{L/R} - \partial_n A_m^{(L/R)} - i[A_m^{L/R}, A_n^{L/R}],$$
$$D_m X = \partial_m X - iA_m^L X + iXA_m^R. \quad (2)$$

In the original version of the soft-wall model, the dilaton field $\Phi$ is chosen to be a simple quadratic form $\Phi(z) = \mu^2 z^2$. By using this parametrization, the calculated meson spectra are consistent with desired linear Regge behavior [47], i.e., $m_n^2 \sim n$. However, it can be shown that there is no spontaneous chiral symmetry breaking in this case [32]. So, this simple quadratic form of dilaton field cannot fulfill our needs.

Note that only the IR behavior of dilaton field can be constrained by the requirement of linear Regge trajectory. Consequently, there remains some freedom to modify the concrete behavior of dilaton field in the UV region.

As pointed out in [32], the specific profile of dilaton field which serves our purpose well can be written as

$$\Phi(z) = -\mu_1^2 z^2 + (\mu_1^2 + \mu_0^2) z^2 \tanh(\mu_2^2 z^2). \tag{3}$$

The nonlinear scalar potential in this model is chosen to be

$$V_X(X) = M_5^2 X^+ X + \lambda |X|^4 + \gamma \mathrm{Re}[\det(X)], \tag{4}$$

with the third term on the right corresponding to the t 'Hooft determinant term. This term is necessary in $SU(3)$ or three flavor case. By adding this term, the chiral phase transition in the chiral limit is shown to be first order [33]. Taking the AdS radius $L = 1$ throughout this work, the 5D mass can be determined by standard AdS/CFT prescription, i.e., $M_5^2 = (\Delta - p)(\Delta + p - 4)$. For the complex scalar field $X$, the 5D mass square is just $M_5^2 = -3$ by taking $\Delta = 3$, $p = 0$.

There are five model parameters in this setup. As in [32], the two parameters in the scalar potential are taken to be

$$v_3 \equiv \frac{2\sqrt{2}}{3}\gamma = -3, \qquad v_4 \equiv \frac{\lambda}{4} = 8, \tag{5}$$

which are determined by the qualitative behavior of chiral phase transition in this model. The remaining three parameters in the dilaton profile (3) are taken to be

$$\mu_0 = 0.43 \text{ GeV}, \quad \mu_1 = 0.83 \text{ GeV}, \quad \mu_2 = 0.176 \text{ GeV}. \tag{6}$$

Here, the value of $\mu_0$ is determined by the slope of the radial excitation of mesons, i.e., $m_n^2 \propto 4\mu_0^2 n$. The value of $\mu_1$ and $\mu_2$ are fixed by the chiral phase transition temperature and the value of chiral condensate at zero temperature for two flavor case. For more details, please refer to [32].

Based on these values of model parameters, we will show the detailed chiral phase transition behavior from this model in the next section.

### B. Chiral phase transition

By using the prescription proposed by Witten [4], the gravity dual of finite temperature system corresponds to introducing a black hole in $AdS_5$.

In this work, we investigate the dynamics of chiral systems at a given temperature. Therefore, this chiral system can be understood as being in thermal equilibrium through interaction with a large heat bath. From this perspective, the gravitational background can be interpreted as providing the desired large heat bath and its dynamics can be approximately neglected. This approximation is just the so-called probe limit. In the probe limit, we simply neglect the backreaction of matter fields to the background metric. Besides, it should be emphasized that, in this specific limit, the possible influence on the gravitational background exerted by the dilaton field is also ignored. As already pointed out in the model setting part, the concrete form of the dilaton field is phenomenologically chosen as the one suited to studying properties related to chiral systems, such as confinement and chiral phase transitions. Thus, the background metric is simply taken to be the AdS-Schwarzschild black hole solution in the Poincaré patch,

$$ds^2 = \frac{1}{z^2}\left[-f(z)dt^2 + \frac{1}{f(z)}dz^2 + dx_i dx^i\right], \tag{7}$$

and

$$f(z) = 1 - \frac{z^4}{z_h^4}, \tag{8}$$

where $z_h$ is the black hole horizon defined by $f(z_h) = 0$. This parameter can be related to the temperature of boundary field theory directly by the following relation

$$T = \left|\frac{f'(z_h)}{4\pi}\right| = \frac{1}{\pi z_h}. \tag{9}$$

In this work, we do not aim to study the detailed mechanisms of the chiral phase transition itself. Instead, we focus on the dynamical properties of the chiral system with nontrivial background chiral condensate. Hence, for simplicity, we choose the case with degenerate three-flavors ($m_q = m_u = m_d = m_s$) and the matrix field $X$ can be naturally parametrized as $X = \chi(z)\mathbf{1}_{3\times 3}/\sqrt{2}$, where $1/\sqrt{2}$ is just a normalization factor in order to make kinetic term canonical.

By substituting the above metric ansatz (7) into the 5D action (1), the equation of motion of field $\chi(z)$ can be obtained by using standard variational method, which is

$$\chi'' + \left(-\frac{3}{z} - \Phi' + \frac{f'}{f}\right)\chi' + \frac{1}{z^2 f}(3\chi - 3v_3\chi^2 - 4v_4\chi^3) = 0, \tag{10}$$

where the prime refers to the derivative with respect to AdS coordinate $z$.

In order to extract the physical information, we need the asymptotic expansion of field $\chi(z)$ near the boundary ($z = 0$). With the equation of motion (10), this can be easily dealt with, and the result is written as

$$\chi(z \to 0) = m_q \zeta z - 3m_q^2 v_3 \zeta^2 z^2 - m_q \zeta [m_q^2(9v_3^2 - 2v_4)\zeta^2 + \mu_1^2] z^3 \log(z) + \frac{\langle \bar{q}q \rangle}{\zeta} z^3 + \mathcal{O}(z^4), \tag{11}$$

where $\zeta = \sqrt{3}/(2\pi)$ is the suitable normalization factor as pointed out by [48]. Thus, the chiral condensate $\sigma = \langle \bar{q}q \rangle$

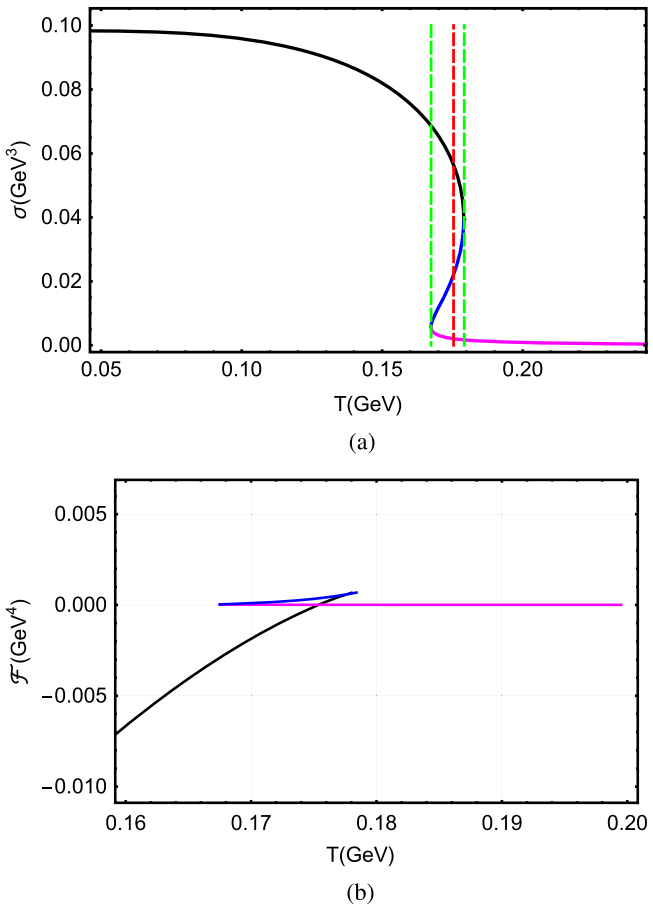


FIG. 1. The typical first order chiral phase transition behavior with quark mass $m_q = 7$ MeV. These results are the same as the previous studies [33]. (a) The temperature dependence of chiral condensate σ. Different color refers to different phase. The green vertical dashed lines mark the domain where multiple phases coexist. The red vertical line marks the transition temperature $T_c = 175.4$ MeV. (b) The calculated free energy densities with quark mass $m_q = 7$ MeV. The color of each curve corresponds exactly to the solution of the same color in the above phase diagram.

can be extracted by solving corresponding equation of motion, when the quark mass $m_q$ is specified.

In Fig. 1(a), we show the temperature dependence of chiral condensate $\sigma$ with the quark mass $m_q = 7$ MeV. In this case, the system shows the clear behavior of first order chiral phase transition, with regions containing multiple phases marked by green vertical dashed lines. By using holographic prescription, the free energy density can be obtained by on-shell bulk action. With a finite quark mass, the on-shell action is divergent at $z = 0$. We need to do holographic renormalization. After subtracting possible divergent terms by suitable holographic renormalization operation, the calculated results of free energy densities of the system are shown in Fig. 1(b). The color of each curve corresponds exactly to the solution of the same color in the phase diagram Fig. 1(a). The transition temperature for this first order phase transition can be identified to be $T_c = 175.4$ MeV from points where the free energy densities are equal. The two green vertical dashed lines mark the domain where multiple phases coexist. The concrete temperature values corresponding to these green dashed lines are $T = 167.4$ MeV and $T = 179.2$ MeV, respectively.

By varying the quark mass, the chiral phase transition evolves from first-order to second-order, and finally becomes a crossover. This phenomenon is consistent with typical prediction made by Columbia plot [1]. Therefore, employing this model enables us to further investigate the associated dynamical properties of systems exhibiting distinct chiral phase transition behaviors. These potential dynamical properties constitute the primary focus of this work and will be further discussed in subsequent sections.

## III. LINEAR PERTURBATION AND QUASINORMAL MODES

Building on the background with varied phase transition behaviors discussed in previous sections, we now examine linear perturbations on the given background.

In this work, we only investigate the scalar mode. Therefore, we decompose the $\chi$ field as follows:

$$\chi(z,t,\boldsymbol{x}) = \chi(z) + \sigma(z,t,\boldsymbol{x}), \tag{12}$$

where $\chi(z)$ is just the background field satisfying equation of motion (10) and $\sigma(z,t,\boldsymbol{x})$ is the perturbation field.

To derive the linearized perturbation equations, we retain terms up to second order in the perturbation field $\sigma$ within the 5D bulk action, which can be written as

$$\begin{aligned} S = -\int d^5x\sqrt{-g}e^{-\Phi}\Big[&\frac{1}{2}g^{MN}\partial_M\sigma\partial_N\sigma + g^{zz}\partial_z\chi\partial_z\sigma \\ &+ (-3\chi + 3v_3\chi^2 + 4v_4\chi^3)\sigma \\ &+ \left(-\frac{3}{2} + 3v_3\chi + 6v_4\chi^2\right)\sigma^2\Big]. \end{aligned} \tag{13}$$

Given that the background field $\chi(z)$ must satisfy its own on-shell condition, the corresponding linearized perturbation equation take the following form:

$$\begin{aligned} 0 = \sigma_k'' - \left[\frac{3}{z} - \frac{f'(z)}{f(z)} + \Phi'(z)\right]\sigma_k' + \left(\frac{\omega^2}{f(z)^2} - \frac{\boldsymbol{k}^2}{f(z)}\right)\sigma_k \\ - \frac{1}{z^2 f(z)}(-3 + 6v_3\chi + 12v_4\chi^2)\sigma_k. \end{aligned} \tag{14}$$

Here, owing to the linear nature of the perturbation equation, modes with different momenta decouple from each other. Consequently, the momentum-space representation of the perturbation field can be safely substituted for

its corresponding coordinate-space field without introducing any inconsistencies.

The corresponding on-shell action will reduce to the boundary term

$$S_{\text{boundary}} \sim -\frac{1}{2}\lim_{z\to 0}\int \frac{d^4k}{(2\pi)^4}[\sqrt{-g}e^{-\Phi}g^{zz}\sigma_k(z)\partial_z\sigma_k(z)] + \text{contact terms}. \tag{15}$$

On the other hand, the solution obeying the incoming boundary condition at the horizon can be written as

$$\sigma_k(z) = s_1(k)z(1+\cdots) + s_3(k)z^3(1+\cdots). \tag{16}$$

In holographic duality, the perturbation field $\sigma$ couples to some particular operator $\mathcal{O}$ of the dual field theory at the boundary. Then, by applying the Lorentzian AdS/CFT prescription developed in [12] to the on-shell action (15), the retarded correlator can be given by

$$G^R(k) \equiv \langle \mathcal{O}(k)\mathcal{O}(-k)\rangle_R \sim \frac{s_3(k)}{s_1(k)} + \text{contact terms}. \tag{17}$$

Consequently, the poles of retarded correlator correspond to zeros of the function $s_1(k)$. It should be emphasized that when solving the perturbation equation (14), incoming boundary condition must be imposed at the horizon. This is equivalent to basic definition of quasinormal modes. In other words, condition $s_1(k) = 0$ actually defines the spectrum of quasinormal modes for scalar perturbations. This statement was first pointed also by [12]. The real and imaginary parts of the quasinormal frequencies can be mapped to the pole masses and the thermal widths of particles excited from the hot medium [41,49–52].

For the convenience of forthcoming analysis, we also define the corresponding spectral function as

$$\rho(k) = -2\,\mathrm{Im}\,G^R(k), \tag{18}$$

which is a commonly used definition.

In summary, we will use the framework outlined above, calculate the quasinormal spectrum and retarded correlator (more precisely, spectral function) with given background configurations.

## IV. DYNAMICAL INSTABILITY IN THE SPINODAL REGION

Inspired by Gubser and Mitra [15,16], systems with thermodynamic instability may induce possible dynamic instability. Based on the previous introduction, we can construct a system exhibiting first-order chiral phase transition behavior using the nonlinear soft-wall model, its phase diagram is already shown in Fig. 1. Note that a hallmark of first-order phase transitions is the existence of thermodynamically unstable solution within their spinodal region. The basic schematic picture is shown in Fig. 2. Thus, we can use current model to study possible dynamical instability induced by thermodynamic instability directly. In this section, we will discuss such dynamical instability in the spinodal region, either at linear perturbation level or at fully nonlinear evolution level.

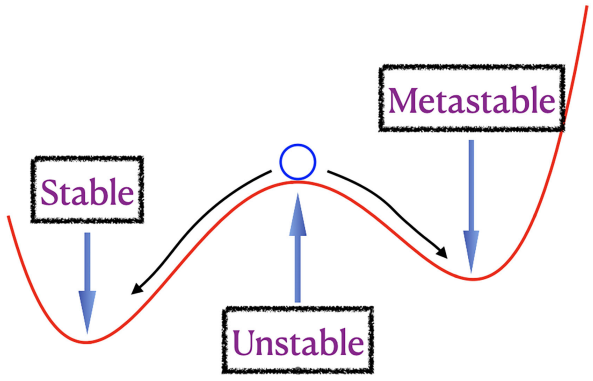


FIG. 2. The schematic picture of a typical first-order phase transition in the spinodal region. The red curve represents the usual thermodynamic potential of system of interest. The thermodynamically unstable solution refers to the local maximum of this potential.

### A. Linear dynamical instability from quasinormal modes

At the linear level, the dynamical properties of a certain system can be well described by its quasinormal modes. In general, during the initial transient regime, the nonequilibrium evolution of a system exhibits significant sensitivity to initial conditions and thus fails to reveal its intrinsic dynamic properties. Consequently, we focus on the long-time behavior, and equivalently, the lowest quasinormal mode in the whole spectrum. Physically, the inverse of the frequency of such lowest quasinormal mode can be interpreted as the upper bound of thermalization time of a given system.

Typically, the time dependent behavior of certain mode can be approximately described by $e^{-i\omega t}$, especially in the long-time regime. Remember that the frequencies of quasinormal modes are complex numbers. Thus, in the analysis based on quasinormal modes, if the frequency of a quasinormal mode has a positive imaginary part, then the corresponding mode will exhibit exponential temporal growth $\sim e^{|\,\mathrm{Im}[\omega]|t}$, inducing system instability that culminates in fragmentation. On the contrary, those perturbation modes with negative imaginary part will decay exponentially and lead the system relax back to the given background solution. Hence, we adopt the presence of quasinormal modes with positive imaginary parts as the criterion for determining system dynamical stability under linear perturbations.

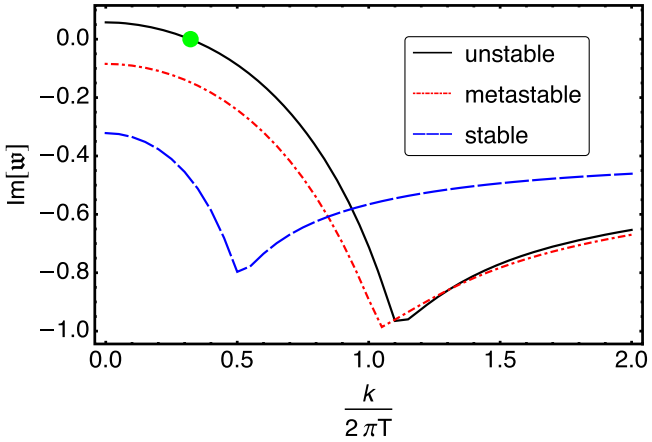


FIG. 3. The imaginary part of normalized frequency $\mathfrak{w} = \omega/2\pi T$ of lowest QNM as a function of dimensionless spatial momentum $k/2\pi T$ with respect to three different background solutions at $T = 173.3$ MeV. The large green dot refers to the position corresponding to the critical momentum $k_c = 0.32(2\pi T) = 348.4$ MeV.

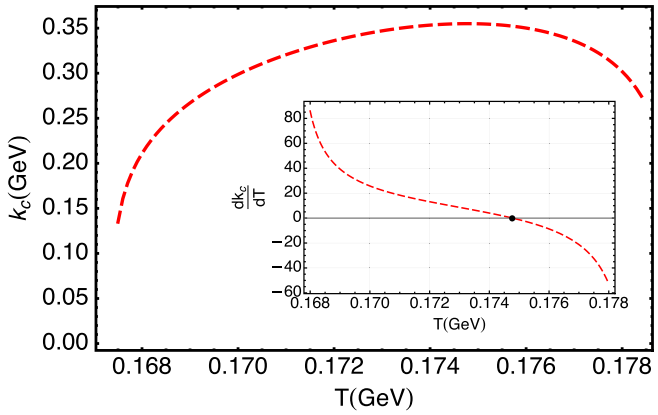


FIG. 4. The temperature dependence of critical momentum $k_c$. The insert shows the derivative of critical momentum with respect to temperature. The black dot in the insert marks the maximum of critical momentum, with temperature $T_{\mathrm{Max}} = 174.8$ MeV.

In Fig. 3, we show the spatial momentum dependence of the imaginary part of lowest quasinormal modes at fixed temperature $T = 173.3$ MeV. All the parameters are normalized to be dimensionless. Compared to Fig. 1, this temperature lies in the spinodal region, and consequently, we have three different background solutions corresponding to different static thermodynamic properties. Clearly, dynamic instability can potentially emerge exclusively from perturbations applied to thermodynamically unstable backgrounds, which is denoted by black line in Fig. 3. For comparison, for those thermodynamically stable backgrounds, all corresponding quasinormal modes have frequencies with negative imaginary parts, which physically correspond to dynamically stable perturbations. This result agrees with our expectation based on Gubser-Mitra conjecture.

Interestingly, possible dynamic instabilities exist only within finite momentum-space regions. The large green dot in the Fig. 3 marks the position of critical momentum $k_c$, which is 348.4 MeV in this case. Note that physically, the critical momentum corresponds to a critical length scale $l_c \sim 1/k_c$. Thus, the existence of a critical momentum implies that only perturbations with sufficiently large spatial scales ($l > l_c$) can induce dynamic instability to the entire system. As a result, given that small-scale perturbations remain dynamically stable, thermodynamically unstable state retains a degree of stability in some sense. The observation described above shares similar qualitative characteristic with previous studies on Gregory-Laflamme instability [13,14] and spinodal instability of holographic superfluid [53,54]. But it should be emphasized that in the previous studies mentioned above, all perturbation modes were exclusively hydrodynamic modes, satisfying $\lim_{k\to 0}\omega(k) = 0$. In our case, it is obvious that the perturbation modes are all nonhydrodynamic modes. This phenomenon may be interpreted as the consequence of the infinite 't Hooft coupling [55].

Besides, the critical momentum also shows the nontrivial temperature dependence. In Fig. 4, we directly investigate such dependence. Systems with larger critical momentum exhibit greater susceptibility to induced dynamic instability. Consequently, critical momentum $k_c$ may serve as a quantitative measure of the degree of dynamic instability in a given system. In the case studied in this section, the maximum of $k_c$ appears at $T = 174.8$ MeV, which is rather close to the first-order chiral phase transition temperature $T_c = 175.4$ MeV. Owing to this, we conclude that the region near the critical temperature of first-order phase transition can be related to the region with maximal dynamical instability. This observation implies that some dynamical information of the given system may be encoded in some thermodynamic quantities.

### B. Dynamical instability from nonlinear evolution

Although the analysis based on quasinormal modes does provide substantial insights into system dynamical properties, it loses all the effects coming from full nonlinear coupling. In this section, we briefly analyze the dynamical instability by using full nonlinear time dependent evolution. Our purpose is to provide further evidence for the existence of dynamic instability discussed in preceding section.

In general, the bulk geometry with embedding black hole has singularity at the black hole horizon. To avoid such difficulty, suitable coordinate system should be chosen. In this work, we transform to the Eddington-Finkelstein (EF) coordinates, and the corresponding metric can be written as

$$ds^2 = \frac{1}{z^2}[-f(z)dt^2 - 2dtdz + dx^i dx^i]. \tag{19}$$

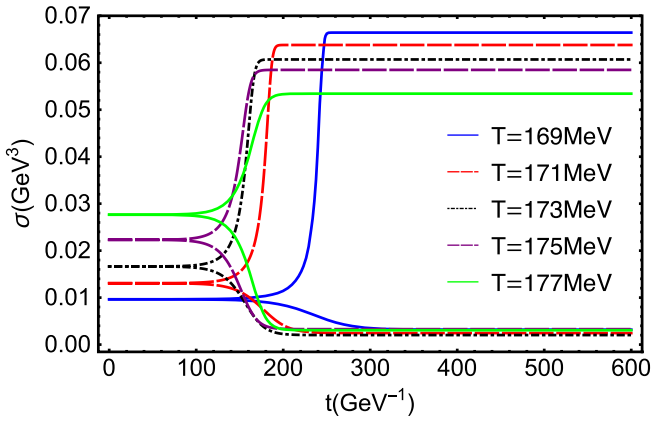


FIG. 5. The nonlinear evolution of chiral condensate $\sigma = \langle \bar{q}q \rangle$ with different temperature. All the background solutions are chosen to be thermodynamically unstable.

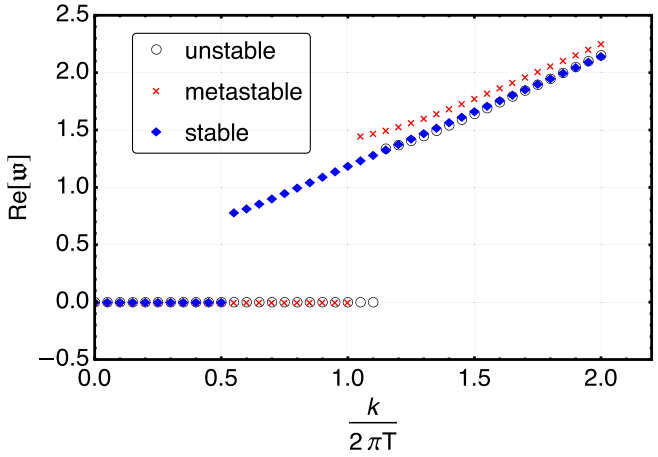


FIG. 6. The real part of normalized frequency $\mathfrak{w} = \omega/2\pi T$ as a function of dimensionless spatial momentum $k/2\pi T$ for three different solutions at $T = 173.3$ MeV.

Here, we use $t$ coordinate as EF time without introducing any ambiguity. The typical advantage is that EF time in bulk reduces to physical time in boundary and remains nonsingular at the horizon.

Empirical insights from linear perturbation theory indicate that large-scale perturbations exhibit heightened propensity to trigger dynamical instability. Thus, in this section, we focus on the perturbations with spatial momentum $\boldsymbol{k} = 0$, which is equivalent to spatially homogeneous perturbations.

In Fig. 5, we show time evolution of chiral condensate at full nonlinear level. These temperatures are chosen to be in the spinodal region of first-order phase transition. The background solution corresponding to each curve is chosen to be the thermodynamically unstable one. We set the typical magnitude of the initial perturbations to be of order $\sim\mathcal{O}(10^{-9})$, which is a rather small value. Even under such tiny perturbations, thermodynamically unstable systems manifest unambiguous phase separation after evolving over sufficient timescales. This is the obvious evidence that the modes corresponding to dynamical instability dominate the long-time evolution behaviors of given systems. In this way, the specific time when the phase separation begins can be treated as the measure of dynamical instability. Consistent with the observation from linear perturbation calculation, systems exhibit progressively earlier onset of phase separation driven by dynamic instability when approaching the first-order transition temperature $T_c$.

In summary, either at linear level or at full nonlinear level, the background with thermodynamical instability do induce dynamical instability. The closer a system approaches the first-order phase transition temperature, the more readily dynamic instability can be triggered.

## V. DIFFUSION-TO-SOUND TRANSITION

Apart from evidence signaling dynamic instability, some more interesting phenomenon can also be observed in Fig. 3. This phenomenon will constitute the primary focus of in-depth examination in this section.

### A. Basic characteristics of the transition

Note that, in Fig. 3, the monotonicity of the imaginary part of lowest quasinormal mode frequencies with respect to spatial momentum exhibits significant alteration. To uncover the underlying physics hidden behind this phenomenon, in Fig. 6, we show the spatial momentum dependence of the real part of lowest quasinormal modes, which are the same modes already shown in Fig. 3.

Compare Fig. 3 with Fig. 6, at the transition point where monotonicity of the frequency's imaginary part changes, the underlying physical process involves mode transition from diffusive mode (with vanishing real part) to propagating mode (with nonzero real part). This means that the property of mode which is dominant in the long-time evolution region has significantly changed. To illustrate, within the long-time evolution regime, perturbations at large spatial scales (corresponding to small momentum regions) can only approach the final state via diffusive processes, whereas at small spatial scales (corresponding to high momentum regions), they can propagate like the usual sound mode.

It should be emphasized that in Fig. 6, at identical temperature, perturbation modes on three distinct thermodynamic background solutions exhibit similar diffusion-to-sound transition behavior. This suggests that this typical transition behaviors are not related to the nature of first-order chiral phase transition. Indeed, we check the situation with larger quark masses, which correspond to usual crossover behaviors, and also observe this particular diffusion-to-sound transition. To simplify, we will investigate the case with the background solution exhibiting crossover behavior and set quark mass $m_q = 40$ MeV in the subsequent discussion. After further detailed investigation, although the aforementioned phenomenon shows no apparent correlation with the

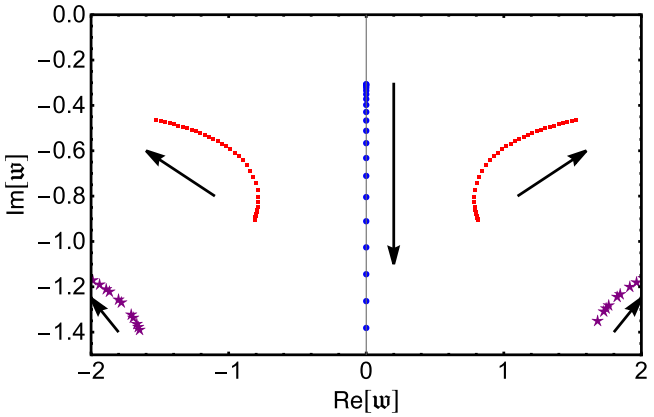


FIG. 7. Evolution of the lowest five quasinormal modes of scalar perturbations in the complex dimensionless frequency $\mathfrak{w} = \omega/2\pi T$ plane. The black arrows show the directions corresponding to the spatial momentum increasing.

specific order of the chiral phase transition, its manifestation is fundamentally linked to chiral symmetry breaking and its restoration.

The information obtained from the lowest QNM only is not complete. One may be misled to conclude that the diffusive modes no longer exist in the large spatial momentum region after the manifestation of diffusion-to-sound transition by observing Fig. 6. This is not exactly the case. To resolve the aforementioned ambiguity, we further study the evolution of the lowest five quasinormal modes in the complex plane as functions of spatial momentum. In Fig. 7, we choose the background temperature to be 240 MeV and plot the desired quasinormal modes in the whole complex plane. The rationale for selecting a relative high background temperature stems from the predominance of propagating modes over diffusive modes within low-temperature regimes. Consequently, to investigate the interplay between diffusive and propagating modes, we strategically designate 240 MeV as the representative background temperature.

In Fig. 7, one direct observation is that the diffusive mode does not simply disappear in the large momentum region. Such mode always manifests itself in the quasinormal spectrum when the chiral system is in high-temperature regime. The fundamental distinction underlying diffusion-to-sound transition lies in the starkly contrasting dependence on spatial momentum exhibited by the imaginary parts of diffusive versus propagating modes. Namely, as spatial momentum increases, the absolute value of the imaginary part of diffusive mode increases, and absolute value of the imaginary part of propagating mode, by contrast, decreases. Consequently, when the spatial momentum exceeds a critical value, the absolute value of the imaginary part becomes greater for diffusive modes than for propagating modes. Typically, the mode with negative imaginary part decays exponentially in time $\sim e^{-|\,\mathrm{Im}[\omega]|t}$. Thus, mode with larger absolute imaginary part experiences faster temporal decay, as a result, such modes ceases to dominate in long-time evolution. To summarize, diffusive mode undergoes rapid decay in high-momentum regimes, thus allowing propagating modes to be dominant in long-time evolution within these momentum domains. This characteristic is captured by the diffusion-to-sound transition observed in Fig. 6.

### B. Spectral functions and transport peak

While our preceding discussion has detailed the fundamental aspects of the diffusion-to-sound transition phenomenon, a thorough exploration of possible underlying physical interpretation has yet to be undertaken. In this section, we calculate corresponding spectral functions and try to give a simple physical picture of such interesting transition.

The basic framework suitable for calculating spectral functions has been already introduced in Sec. III, specific implementation details of the calculations are not reiterated here. But we should emphasize that the corresponding operator we calculate in this section is the scalar operator $\hat{\mathcal{O}}(x) = \bar{q}q(x)$.

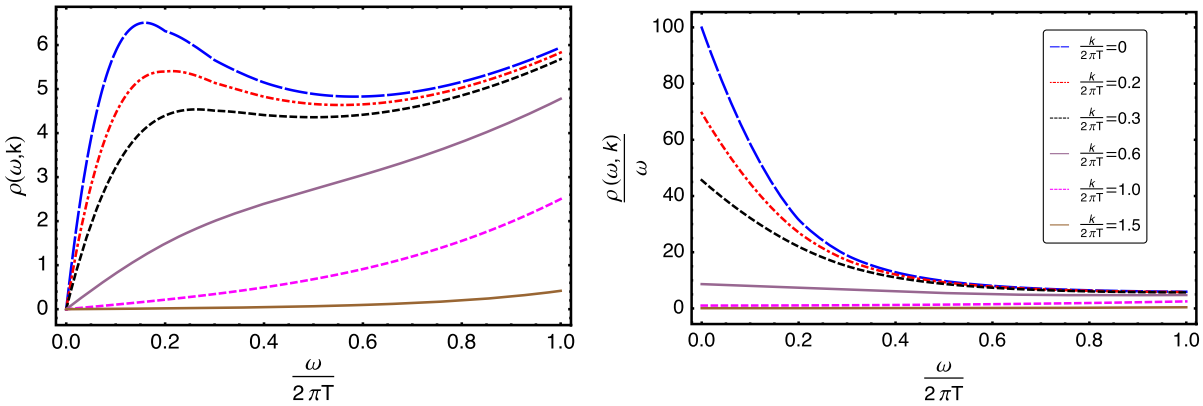


FIG. 8. The spectral function of scalar operator $\hat{\mathcal{O}}(x) = \bar{q}q(x)$ as a function of dimensionless frequency $\omega/2\pi T$ for different spatial momentum. The background temperature is chosen to be 200 MeV. The left panel shows behaviors of the original spectral function $\rho(\omega, k)$ and the right panel shows behaviors of the rescaled spectral function $\rho(\omega, k)/\omega$. The two panels share the same figure legend.

We first investigate the influence of spatial momentum on the spectral functions. To do this, we calculate the desired spectral function $\rho(\omega, k)$ as a function of dimensionless frequency $\mathfrak{w} = \omega/2\pi T$ for different spatial momentum. The results are displayed in Fig. 8. In the right panel of Fig. 8, we rescale the spectral function by a factor $\omega$ in order to elucidate the behavior within the low-frequency region. In this case, a narrow structure known as the transport peak (regarding studies on transport peak, one may consult Refs. [55–57]) rises in the small frequency region. Further, we have moderately expanded the conceptual scope of transport peaks. Typically, the transport peak is defined at zero spatial momentum. In this work, we treat similar peaks appearing in the spectral functions as transport peaks, even though the corresponding spatial momentum $k$ are not zero.

One direct observation is that such narrow peak only exists in the small spatial momentum region, $0 \leq k \leq k_{\max}$. This aligns precisely with the earlier observation from quasinormal mode computations: diffusive modes dominate only within low spatial momentum regions. Clearly, these narrow peaks correspond to such diffusive modes. The correspondence between diffusive modes and transport peak structures in spectral functions has been reported in prior research [55].

Next we examine the influence of temperature on transport peak structure. By investigating the temperature dependence of spectral functions, we aim to establish connections between the emergence of transport peak structures and the breaking/restoration of chiral symmetry. In order to simplify the situation, we restrict our calculation for zero spatial momentum. Our numerical results are displayed in Fig. 9.

When temperature is low, the spectral functions exhibit peaks which satisfy the clear Breit-Wigner distribution form. These signify the presence of bosonic excitation modes in the system exhibiting a well-defined thermal mass and finite thermal width. Remembering the scalar operator $\hat{\mathcal{O}}(x) = \bar{q}q(x)$ we have used in this work, these excitations can be recognized as scalar $\sigma$ meson excitation. Compared with other mesons in thermal medium (for example, $\pi$ meson [40]), scalar $\sigma$ meson demonstrates significantly broader thermal widths, consequently exhibiting shorter lifetimes. With increasing temperature, the background chiral condensate $\langle \bar{q}q \rangle$ is reduced and the broken chiral symmetry tends to restore. Consequently, the thermal width of scalar $\sigma$ meson increases significantly. Because of this, the final fate of thermal $\sigma$ meson is dissociation. In Fig. 9, at $T = 180$ MeV, the spectral function no longer exhibits discernible excitation peaks corresponding to such scalar mesons. This means that at $T = 180$ MeV, the thermal scalar $\sigma$ meson has completely dissociated. Further increasing the temperature reveals intriguing phenomena. In the near zero frequency region, a new peak manifests itself and the height of the peak reaches its maximum value when $T \sim 190$ MeV. This kind of peak is just aforementioned transport peak. This correspondence, where spectral functions exhibit meson excitation peaks at low temperatures

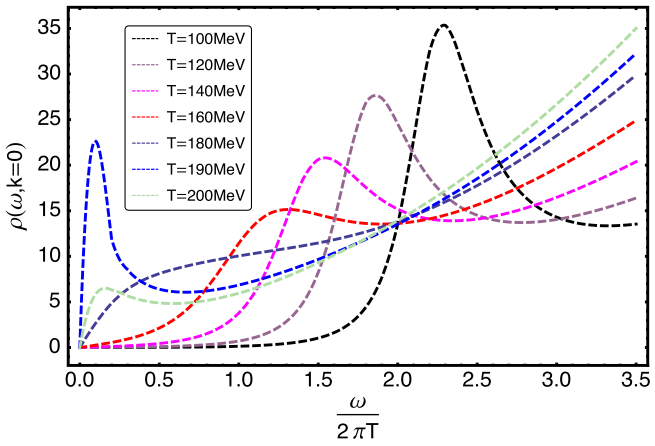


FIG. 9. The temperature dependence of spectral functions as functions of dimensionless $\omega/2\pi T$ for zero spatial momentum.

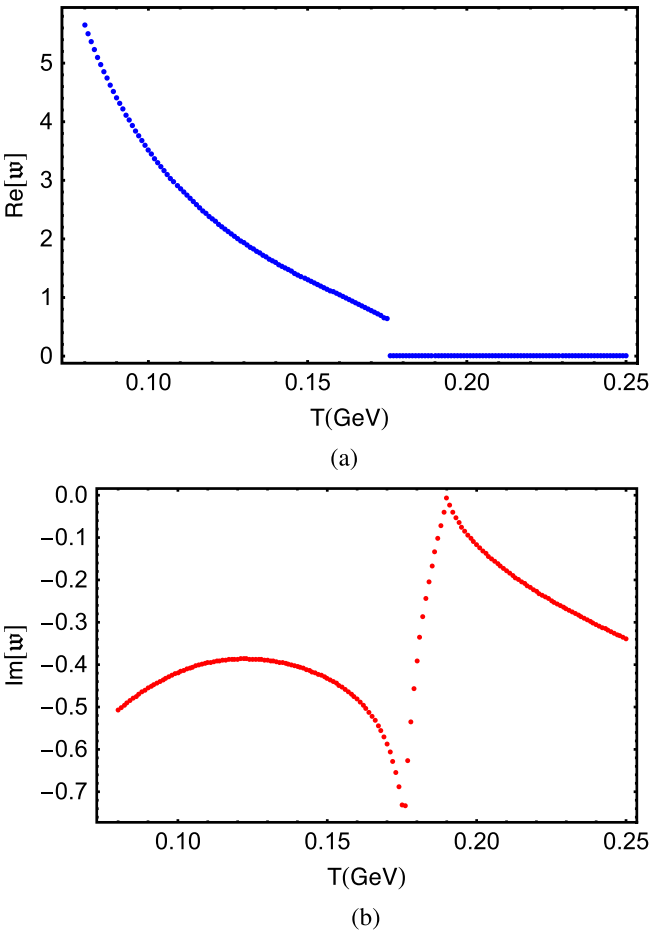


FIG. 10. The temperature dependence of lowest QNM frequency $\mathfrak{w} = \omega/2\pi T$. The spatial momentum $k$ is set to be zero. (a) The temperature dependence of real part of lowest QNM frequency $\mathfrak{w} = \omega/2\pi T$. (b) The temperature dependence of imaginary part of lowest QNM frequency $\mathfrak{w} = \omega/2\pi T$.

but transport peaks at high temperatures, aligns with the temperature-dependent evolution of the lowest quasinormal mode.

To clarify, we show the temperature dependence of the lowest QNM in Fig. 10. We observe that the so-called diffusion-to-sound transition happens at $T_c \approx 175$ MeV. The diffusive modes emerge in the quasinormal mode spectrum exclusively above this critical temperature $T_c$. Obviously, this is consistent with the evolution behavior of spectral functions under temperature changing. Interestingly, the imaginary part of lowest QNM increases with temperature in particular temperature region 175 MeV $\leq T \leq$ 190 MeV. In this region, the height of the transport peak also increases. Accordingly, at $T = 190$ MeV, the amplitude of transport peak attains its maximum value. Further, the spectral functions in the region 180 MeV $\leq T \leq$ 200 MeV are shown in Fig. 11. Within this specific temperature range, the temperature dependence of the transport peak amplitude exhibits parallel evolution with the imaginary part of the lowest quasinormal mode.

In summary, the emergence of transport peaks in spectral functions occurs subsequent to the complete dissociation of corresponding scalar $\sigma$ meson excitations, while concurrently, diffusive modes become the governing modes for long-time evolution within the quasinormal mode spectrum. Naturally, the dissociation of scalar $\sigma$ mesons occurs during partial restoration of chiral symmetry, specifically, when the value of the background chiral condensate falls below a critical threshold, the chiral system ceases to support such mesonic excitations. After the complete dissociation, the basic degrees of freedom of chiral system can be identified as light quarks moving in the thermal medium. Of course, possible gluon contributions should be considered in a thorough investigation, but in this work, we only study contributions from operator constructed by fermionic fields. Further, considering that in prior discussions regarding spatial momentum effects, diffusive modes dominate only for large-scale perturbations. All these fundamental properties indicate that such diffusive modes ultimately emanate from dissipative effects caused by the coupling between nonzero background chiral condensate $\langle \bar{q}q \rangle$ and the propagating quarks in the medium. From this perspective, the occurrence of the diffusion-to-sound transition should depend solely on the concrete value of the background chiral condensate, thus its observed independence from the specific order of any potential chiral phase transition is justified. From another perspective, in Fig. 11, upon further temperature increasing (for instance, $T > 190$ MeV), the transport peak begins to diminish. This occurs because further temperature increasing progressively restores chiral symmetry, diminishing the background chiral condensate and thereby reducing the dissipative effects that impede light quark propagation.

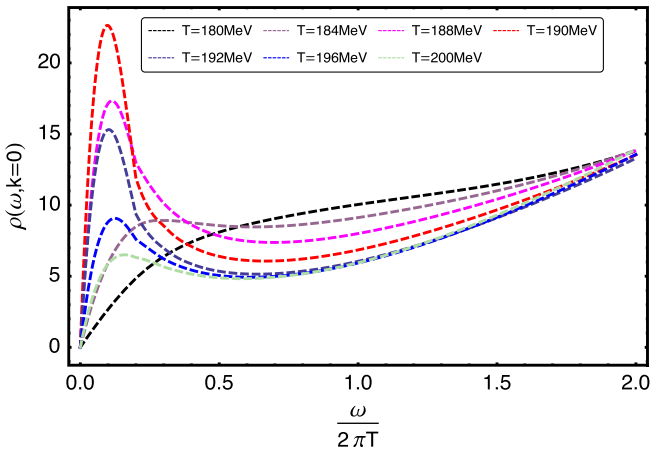


FIG. 11. The temperature dependence of spectral functions as functions of dimensionless $\omega/2\pi T$ for zero spatial momentum in specific temperature region, 180 MeV $\leq T \leq$ 200 MeV.

## VI. SUMMARY AND DISCUSSION

In this work, based on a holographic model, we examine the existing of possible dynamical instability in the spinodal region of first-order phase transition. According to the calculated QNM results, the dynamical instability only appears with respect to the background which lacks thermodynamical instability. A defining characteristic of such dynamical instability is that it manifests only within the low-momentum regime, i.e., $0 \leq k \leq k_c$. This critical momentum $k_c$ serves as a quantitative measure of the magnitude of dynamical instability. Moreover, critical momentum $k_c$ shows nontrivial temperature dependence. It follows that the region near the first-order phase transition temperature exhibits maximal dynamical instability. These results are consistent with the behavior derived from nonlinear real-time dynamical evolution.

An intriguing additional finding is that the lowest quasinormal mode undergoes a diffusion-to-sound transition in some temperature region. This means that the dominant mode governing the system's long-time evolution undergoes a transition. As can be seen, diffusive modes only dominate for the perturbations in large spatial scale. When the diffusive mode becomes dominant, the corresponding spectral function exhibits a distinct transport peak. Considering the influence of temperature, we see that the transport peak begins to emerge after complete dissociation of scalar $\sigma$ meson. We argue that this transition phenomenon can be elucidated through the dissipative effects engendered by a nonzero background chiral condensate $\langle \bar{q}q \rangle$. Based on such interpretation, diffusion-to-sound transition can be related to chiral symmetry breaking and restoration. Besides, it should be emphasized that this transition is independent of the specific order of the chiral phase transition.

Although in this work we refer to the narrow peak structure emerging in the low-frequency region of the spectral function as the transport peak, its conventional interpretation remains intrinsically linked to specific transport coefficients.

For instance, the spectral function $\rho_{xy,xy}(\omega, q)$ of energy-momentum tensor $T_{xy}$ can be related to shear viscosity $\eta$ by the formula (see, e.g., [55])

$$\rho_{xy,xy}(\omega, 0) = 2\eta\omega + \mathcal{O}(\omega^3). \tag{20}$$

Unfortunately, such a relation has yet to be established in this work. Generally, the dynamics of heavy quarks can be adequately described through classical diffusive processes because of large masses, whereas light quarks exhibit highly relativistic motion that cannot be typically captured by classical approximations. In this work, we investigate light quark system where the manifestation of a diffusive mode in the quasinormal mode spectrum emerges as an entirely unexpected phenomenon. Whether a diffusion coefficient analogous to that for heavy quark system can be meaningfully introduced for light quark matter under such circumstances remains an open question. We aim to resolve through subsequent investigations.

In this work, we investigate the various dynamical properties of chiral system which interacts with some large heat bath. We are not concerned with certain physical effects associated with gravitational dynamics, such as entropy production and temperature fluctuations of the system. Accordingly, the corresponding metric can be approximately chosen to be the static AdS-Schwarzschild black hole solution. Based on this approximation, We are able to analyze the differences in dynamical stability among the distinct phases present in the chiral system at a given temperature. However, such an approximation is only suitable for addressing the specific problem investigated in this work and does not fully capture the complete dynamical properties of the chiral system. In principle, the complete dynamic information should incorporate the part deriving from the gravitational field. It is not immediately obvious whether relaxing the aforementioned approximation and incorporating full gravitational effects would lead to qualitatively significant differences in the results of this work. The final answer to this question can only be obtained by fully solving the self-consistent equations of motion. Despite significant progress having been made in the study of dynamical gravitational fields [58–62], research involving the coupling of various matter fields remains scarce, constrained by the technical challenges in solving the equations of motion that include gravitational sector. Notwithstanding the technical challenges outlined above, addressing them constitutes a worthwhile undertaking. We hope to address this issue in our future studies.

## ACKNOWLEDGMENTS

We thank Yi Lu for his helpful discussion. This work is supported by the National Natural Science Foundation of China (NSFC) Grants No. 12305136, No. 12275108, No. 12235016, No. 12221005, No. 12247107, No. 12175007, the start-up funding of Hangzhou Normal University under Grant No. 4245C50223204075, and the Fundamental Research Funds for the Central Universities.

## DATA AVAILABILITY

The data that support the findings of this article are not publicly available upon publication because it is not technically feasible and/or the cost of preparing, depositing, and hosting the data would be prohibitive within the terms of this research project. The data are available from the authors upon reasonable request.

[1] C. S. Fischer, QCD at finite temperature and chemical potential from Dyson–Schwinger equations, Prog. Part. Nucl. Phys. **105**, 1 (2019).
[2] N. Dupuis, L. Canet, A. Eichhorn, W. Metzner, J. M. Pawlowski, M. Tissier, and N. Wschebor, The nonperturbative functional renormalization group and its applications, Phys. Rep. **910**, 1 (2021).
[3] E. Witten, Anti de Sitter space and holography, Adv. Theor. Math. Phys. **2**, 253 (1998).
[4] E. Witten, Anti-de Sitter space, thermal phase transition, and confinement in gauge theories, Adv. Theor. Math. Phys. **2**, 505 (1998).
[5] J. M. Maldacena, The Large *N* limit of superconformal field theories and supergravity, Adv. Theor. Math. Phys. **2**, 231 (1998).
[6] S. S. Gubser, I. R. Klebanov, and A. M. Polyakov, Gauge theory correlators from noncritical string theory, Phys. Lett. B **428**, 105 (1998).
[7] O. Aharony, S. S. Gubser, J. M. Maldacena, H. Ooguri, and Y. Oz, Large N field theories, string theory and gravity, Phys. Rep. **323**, 183 (2000).
[8] E. Berti, V. Cardoso, and A. O. Starinets, Quasinormal modes of black holes and black branes, Classical Quantum Gravity **26**, 163001 (2009).
[9] P. K. Kovtun and A. O. Starinets, Quasinormal modes and holography, Phys. Rev. D **72**, 086009 (2005).
[10] A. O. Starinets, Quasinormal modes of near extremal black branes, Phys. Rev. D **66**, 124013 (2002).
[11] G. T. Horowitz and V. E. Hubeny, Quasinormal modes of AdS black holes and the approach to thermal equilibrium, Phys. Rev. D **62**, 024027 (2000).
[12] D. T. Son and A. O. Starinets, Minkowski space correlators in AdS/CFT correspondence: Recipe and applications, J. High Energy Phys. 09 (2002) 042.
[13] R. Gregory and R. Laflamme, Black strings and p-branes are unstable, Phys. Rev. Lett. **70**, 2837 (1993).

[14] R. Gregory and R. Laflamme, The instability of charged black strings and p-branes, Nucl. Phys. **B428**, 399 (1994).
[15] S. S. Gubser and I. Mitra, Instability of charged black holes in anti-de Sitter space, Clay Math. Proc. **1**, 221 (2002).
[16] S. S. Gubser and I. Mitra, The evolution of unstable black holes in anti-de Sitter space, J. High Energy Phys. 08 (2001) 018.
[17] A. Buchel, A holographic perspective on Gubser-Mitra conjecture, Nucl. Phys. **B731**, 109 (2005).
[18] T. Hirayama, G. Kang, and Y. Lee, Classical stability of charged black branes and the Gubser-Mitra conjecture, Phys. Rev. D **67**, 024007 (2003).
[19] U. Miyamoto, Analytic evidence for the Gubser-Mitra conjecture, Phys. Lett. B **659**, 380 (2008).
[20] H. S. Reall, Classical and thermodynamic stability of black branes, Phys. Rev. D **64**, 044005 (2001).
[21] G. D. Moore, Numerical studies of QGP instabilities and implications, Eur. Phys. J. A **29**, 53 (2006).
[22] P. B. Arnold and G. D. Moore, QCD plasma instabilities: The non-Abelian cascade, Phys. Rev. D **73**, 025006 (2006).
[23] P. B. Arnold and G. D. Moore, The turbulent spectrum created by non-Abelian plasma instabilities, Phys. Rev. D **73**, 025013 (2006).
[24] A. Kurkela and G. D. Moore, Bjorken flow, plasma instabilities, and thermalization, J. High Energy Phys. 11 (2011) 120.
[25] S. Nakamura, H. Ooguri, and C.-S. Park, Gravity dual of spatially modulated phase, Phys. Rev. D **81**, 044018 (2010).
[26] H. Ooguri and C.-S. Park, Spatially modulated phase in holographic quark-gluon plasma, Phys. Rev. Lett. **106**, 061601 (2011).
[27] H. Ooguri and C.-S. Park, Holographic end-point of spatially modulated phase transition, Phys. Rev. D **82**, 126001 (2010).
[28] T. Demircik, N. Jokela, M. Jarvinen, and A. Piispa, Is holographic quark-gluon plasma homogeneous?, arXiv: 2405.02392.
[29] J. Cruz Rojas, T. Demircik, and M. Järvinen, Modulated instabilities and the AdS2 point in dense holographic matter, Phys. Rev. D **111**, 046017 (2025).
[30] J. Erlich, E. Katz, D. T. Son, and M. A. Stephanov, QCD and a holographic model of hadrons, Phys. Rev. Lett. **95**, 261602 (2005).
[31] A. Karch, E. Katz, D. T. Son, and M. A. Stephanov, Linear confinement and AdS/QCD, Phys. Rev. D **74**, 015005 (2006).
[32] K. Chelabi, Z. Fang, M. Huang, D. Li, and Y.-L. Wu, Chiral phase transition in the soft-wall model of AdS/QCD, J. High Energy Phys. 04 (2016) 036.
[33] D. Li and M. Huang, Chiral phase transition of QCD with $N_f = 2 + 1$ flavors from holography, J. High Energy Phys. 02 (2017) 042.
[34] J. Chen, S. He, M. Huang, and D. Li, Critical exponents of finite temperature chiral phase transition in soft-wall AdS/QCD models, J. High Energy Phys. 01 (2019) 165.
[35] A. Ballon-Bayona, S. Bartz, L. A. H. Mamani, and D. M. Rodrigues, Chiral transition and meson melting within improved holographic soft wall models, Phys. Rev. D **111**, 026011 (2025).
[36] S. P. Bartz, R. C. Meadows, and G. Brock, Chiral phase transition in soft-wall AdS/QCD with scalar-dilaton coupling, Phys. Rev. D **110**, 026027 (2024).
[37] Z. Fang, Y.-L. Wu, and L. Zhang, Chiral phase transition with $2 + 1$ quark flavors in an improved soft-wall AdS/QCD Model, Phys. Rev. D **98**, 114003 (2018).
[38] D. M. Rodrigues, D. Li, E. Folco Capossoli, and H. Boschi-Filho, Chiral symmetry breaking and restoration in $2 + 1$ dimensions from holography: Magnetic and inverse magnetic catalysis, Phys. Rev. D **98**, 106007 (2018).
[39] H. A. Ahmed, M. Kawaguchi, and M. Huang, Effect of charm quark on chiral phase transition in $N_f = 2 + 1 + 1$ holographic QCD, Phys. Rev. D **110**, 046002 (2024).
[40] X. Cao, M. Baggioli, H. Liu, and D. Li, Pion dynamics in a soft-wall AdS-QCD model, J. High Energy Phys. 12 (2022) 113.
[41] X. Cao, S. Qiu, H. Liu, and D. Li, Thermal properties of light mesons from holography, J. High Energy Phys. 08 (2021) 005.
[42] X. Cao, H. Liu, and D. Li, Pion quasiparticles and QCD phase transitions at finite temperature and isospin density from holography, Phys. Rev. D **102**, 126014 (2020).
[43] D. T. Son and M. A. Stephanov, Pion propagation near the QCD chiral phase transition, Phys. Rev. Lett. **88**, 202302 (2002).
[44] X. Cao, J. Chao, H. Liu, and D. Li, Thermalization and prethermalization in the soft-wall AdS/QCD model, Phys. Rev. D **107**, 086001 (2023).
[45] P. Zheng, Y. Chen, D. Li, M. Huang, and Y. Liu, Non-equilibrium dynamics of Goldstone excitation from holography, J. High Energy Phys. 07 (2025) 029.
[46] F. Giannuzzi and S. Nicotri, Out-of-equilibrium chiral condensate in AdS/QCD, Phys. Rev. D **112**, 014039 (2025).
[47] P. D. B. Collins, *An Introduction to Regge Theory and High Energy Physics* (Cambridge University Press, Cambridge, England, 1977).
[48] A. Cherman, T. D. Cohen, and E. S. Werbos, The chiral condensate in holographic models of QCD, Phys. Rev. C **79**, 045203 (2009).
[49] A. S. Miranda, C. A. Ballon Bayona, H. Boschi-Filho, and N. R. F. Braga, Black-hole quasinormal modes and scalar glueballs in a finite-temperature AdS/QCD model, J. High Energy Phys. 11 (2009) 119.
[50] H. R. Grigoryan, P. M. Hohler, and M. A. Stephanov, Towards the gravity dual of quarkonium in the strongly coupled QCD plasma, Phys. Rev. D **82**, 026005 (2010).
[51] L. A. H. Mamani, A. S. Miranda, H. Boschi-Filho, and N. R. F. Braga, Vector meson quasinormal modes in a finite-temperature AdS/QCD model, J. High Energy Phys. 03 (2014) 058.
[52] N. R. F. Braga and L. F. Ferreira, Quasinormal modes for quarkonium in a plasma with magnetic fields, Phys. Lett. B **795**, 462 (2019).
[53] X. Zhao, Z.-Y. Nie, Z.-Q. Zhao, H.-B. Zeng, Y. Tian, and M. Baggioli, Dynamical evolution of spinodal decomposition in holographic superfluids, J. High Energy Phys. 02 (2024) 184.
[54] Z.-Q. Zhao, X.-K. Zhang, and Z.-Y. Nie, Dynamical stability from quasi normal modes in 2nd, 1st and 0th order

holographic superfluid phase transitions, J. High Energy Phys. 02 (2023) 023.

[55] J. Casalderrey-Solana, S. Grozdanov, and A. O. Starinets, Transport peak in the thermal spectral function of $\mathcal{N} = 4$ supersymmetric Yang-Mills plasma at intermediate coupling, Phys. Rev. Lett. **121**, 191603 (2018).

[56] P. Petreczky and D. Teaney, Heavy quark diffusion from the lattice, Phys. Rev. D **73**, 014508 (2006).

[57] G. Aarts and J. M. Martinez Resco, Transport coefficients, spectral functions and the lattice, J. High Energy Phys. 04 (2002) 053.

[58] P. M. Chesler and L. G. Yaffe, Horizon formation and far-from-equilibrium isotropization in supersymmetric Yang-Mills plasma, Phys. Rev. Lett. **102**, 211601 (2009).

[59] P. M. Chesler and L. G. Yaffe, Numerical solution of gravitational dynamics in asymptotically anti-de Sitter spacetimes, J. High Energy Phys. 07 (2014) 086.

[60] A. Kurkela, W. van der Schee, U. A. Wiedemann, and B. Wu, Early- and late-time behavior of attractors in heavy-ion collisions, Phys. Rev. Lett. **124**, 102301 (2020).

[61] M. P. Heller, D. Mateos, W. van der Schee, and D. Trancanelli, Strong coupling isotropization of non-Abelian plasmas simplified, Phys. Rev. Lett. **108**, 191601 (2012).

[62] C. Ecker, E. Kiritsis, and W. van der Schee, Dynamical inflaton coupled to strongly interacting matter, Phys. Rev. Lett. **130**, 251001 (2023).